[UCI]I804:48009-200000501009

Master of Science

Ni doped MoS_2 for catalytic CO oxidation: a DFT study

The Graduate School

of the University of Ulsan

Department of Physics

Md Maruf Mridha

Ni doped MoS_2 for catalytic CO oxidation: a DFT study

Supervisor: Prof. Young-Han Shin

This dissertation is submitted to University of Ulsan in partial fulfillment of the requirements for the degree of

Master of Science in physics

by

Md Maruf Mridha

Department of Physics

University of Ulsan

June, 2021

University of Ulsan
Department of Physics

This dissertation, "Ni doped MoS_2 for catalytic CO oxidation: a DFT study" is hereby approved in partial fulfillment of the requirements for the degree of Master of Science in physics.

Prof. Shinuk Cho
Department of Physics, University of Ulsan

Prof. Sooncheol Hong
Department of Physics, University of Ulsan

Prof. Young-Han Shin
Department of Physics, University of Ulsan

To my all well-wishers.

Declaration

I hereby declare that except where specific reference is made to the work of others, the contents of this dissertation are original and have not been submitted in whole or in part for consideration for any other degree or qualification in this, or any other university.

Md Maruf Mridha
June 30, 2021

Acknowledgements

First of all, I praise my lord Allah (SWT) for his profound kindness and countless blessings, and for helping me to accomplish this work successfully.

Then, I would like to express my heartfelt gratitude to my supervisor Prof. Dr. Young-Han Shin for giving me the opportunity to work in the Multiscale Materials Modeling Lab. at the University of Ulsan. I was lucky enough that my professor allowed me to work on my own freedom, which is the most crucial thing on the way of becoming an independent researcher. I am also grateful to him for his tireless support to develop the research attitude to a novice researcher like me slowly but successfully.

Next, it comes about my two labmates Asad Ali and Dr. Hamid Ullah to whom I owe a lot. After joining this lab, I learned almost everything about the computational basics from them. I never found them unwilling to help me, not for a single time. I am also thankful to my other labmates Seong Boo Park, Pham Thi Hue, Loan Thi Xuan Doan, Than Thi Lien Pham for their help throughout this journey.

I also want to thank my country fellows at the University of Ulsan with whom I had a wonderful time. Among them I like to mention Nazim Uddin, Raziul Islam, Niaz Morshedul Haque, Jashim Uddin Shehab who never let me feel alone in this foreign land.

Finally, very special thanks to my parents for the sacrifice they made by letting their one and only son go for study thousands of miles away from home, and for their continuous prayer and mental support for my success.

Abstract

The investigation of CO oxidation on Ni doped MoS_2 is performed by the means of first principles calculation. The substituted Ni atom with high binding energy of 4.23 eV and high diffusion barrier of 1.95 eV indicates that introducing a dopant atom could make a strong bond and bind stably with monolayers which, subsequently, can be used as a single atom catalyst. Both the LH and ER mechanisms are comparably studied, however, the reaction process is proceed only through the LH mechanism with a two step route ($CO + O_2 \longrightarrow OOCO \longrightarrow CO_2 + O$ and $O + CO \longrightarrow CO_2$) facing energy barrier of 0.79 eV and 0.21 eV, respectively. The low energy barrier in LH mechanism shows the good catalytic behavior of Ni doped MoS_2. This study proposes that the doping of a non-noble metal atom on a chemically inactive monolayer like MoS_2 could be a promising way to get a low cost single atom catalyst for further studies.

Contents

List of Figures

List of Tables

Chapter 1

Introduction

1.1 Historical background of catalysis

In the beginning of the 19th century, researchers observed a number of chemical reactions were occurring in the presence of trace amounts of substances which themselves were not consumed in the reaction. An initiative was taken to bring these observations into the body of chemical knowledge, by a Swedish scientist J.J. Berzelius in 1836, by naming the action catalysis after addressing their behavior as their catalytic power. He said "Catalytic power means that substances are able to awake affinities that are asleep at the temperature by their mere presence." The word "catalysis" comes from the Greek language and means 'breaking down'. Berzelius applied this term to phenomena where the normal barriers from the chemical reactions were removed. According to Ostwald "a substance that increases the rate at which a chemical system approaches equilibrium, without being consumed in the process is called a catalyst". Catalysis is divided into three categories: homogeneous catalysis where the reacting species and the catalyst are in the same phase, in heterogeneous catalysis reacting species and catalyst are in different phases, and biological catalysts called enzymes are related to living things. Catalysts are widely used in industries nowadays. It not only lowers the cost of production, but also the time of production of certain chemical

species, thereby making the product as efficient as possible. Study finds that catalysts are being used at some stage in the process of manufacture of almost 90% of all commercially produced chemical products. From the field of energy processing to the field of environmental protection catalysts play an important role.

1.2 Principle of catalysis

A cyclic process consisting of at least three basic steps: adsorption of the reactants on the catalytic surface, reaction on the surface and desorption of the products is a heterogeneous catalytic process. By influencing kinetics, rather than thermodynamics, the catalyst increases the rate of the chemical reaction. The initial and final state of the reaction remains energy-sensitive, which suggests that the balance between reactants and products does not change in the presence of a catalyst [1]. The same reaction in the gas phase does happen much quicker as the activation barrier in the catalyzed process is substantially lower. The reaction that uses the catalyst becomes more cost effective because it occurs under milder conditions. To make the catalyst successful, the strength of the interaction between reactants and products with a catalyst is crucial. In cases of weak interaction, the molecular bonds cannot be disrupted by the catalytic surface, on the other hand, strong interaction leads to catalyst poisoning. This is called the Sabatier principle. Moderate bonding energies (usually in the range of 0.5 to 1.5 eV), therefore, are optimal for molecules. Catalysis therefore means having the appropriate species on the right surface, at the correct coverage and at the right reaction temperature. These are the essential components, and this concept could be used as a design criterion for catalyst development.

1.3 Ni catalyst

The developement of more and more catalysts is required for the increasing growth of industrial production. The expensive noble metal catalysts can be replaced by the non-noble metal catalysts like Nickel (Ni), although each catalyst has its unique physical and chemical characteristics towards catalytic transformation. Ni has unique characteristics: cheap, environmentally benign, readily available and rich in earth. Having particular interest an observation was made about nickel by famous chemist and Nobel Laureate Paul Sabatier: " It can be compared to a spirited horse, delicate, difficult to control, and incapable of sustainable work." So, like the gold catalyst, Ni was also under a probe for long-time whether it can be used for desired synthetic work. Recent work shows the evidence of Ni as a good catalyst in various fields. The key advantages of Ni are as follows

1. High performance in reactions for which other metals were not efficient;
2. Large variability of electronic states – Ni(0)/Ni(I)/Ni(II)/Ni(III);
3. New reactions and transformation beyond the known limits of other metals;
4. Facile activation and transformation of molecules that are chemically less reactive;
5. Excellent opportunities in photocatalytic and hybrid catalytic cycles.

1.4 CO oxidation : background & studies

Carbon monoxide (CO) is believed to be one of the most hazardous gases in the environment produced due to the incomplete combustion in the fuel cell. Though, back in the mid 2000s, the mass production of vehicles powered by the internal combustion engine brought excellent personal mobility, the major source of man-made urban emissions were not undiscovered. The

oxidation of fuel to carbon dioxide and water was incomplete. Unburnt hydrocarbons and partially combusted products, particularly carbon monoxide (CO), were present at the exhaust gases. This problem emerged as intensive research which led to CO conversion into less harmful products like CO_2 by developing suitable catalysts.

In the field of heterogeneous catalysis, CO oxidation is one of the most extensively studied reactions, and it is reported that the low-temperature CO oxidation has been made a considerable progress in the area of environmental protection and fuel cell industry [2–15]. Though, noble metals (Pt [3, 5], Pd [13, 16, 17], Au [14, 18, 19], Rh [20, 21]) are found efficient towards CO oxidation and the efficiency soars dramatically when the size of the catalysts are brought to nanoparticles or even single atoms [2, 4, 22, 23], often requirements of high temperature to operate and higher prices due to unavailibility in nature are major drawbacks to use the noble metals for the large-scale production. Therefore, finding suitable catalysts which can operate at low temperature, are cost effective and highly efficient for wide applications is a great challenge.

Studies found that supported metal catalysts are excellent for catalytic CO oxidation and results are quite distinguishable from their bulk counterparts. Nonetheless, only small number of atoms act as active sites limit their usage [24]. Therefore, single atom catalyst (SAC) could be superior in the field of heterogeneous catalysis due to their low dimensionality resulting electronic confinement effects of low coordinated metal atoms, and the maximization of atomic efficiency [25]. First reported SAC, Pt supported FeO_x showed good catalytic activity for CO oxidation [26]. Later studies, Fe on graphene , Pt supported MoS_2 [4], Pt supported on phthalocyanine [27] support the idea of SAC based two dimensional materials are effective.

However, in practice, single atom catalyst is too active and mobile. Thus, preparing a SAC with supporting material for wide range of applications in

the field of heterogeneous catalysis is remained a challenge. Hence, introducing a dopant atom or embedding a single atom to the substrate may avoid this problem with the enhancement of the reaction activity. Graphene, a one-atom-thick carbon sheet, has long been studied due to its excellent physical and chemical properties and regarded as a promising candidate for next generation electronic materials. Creating vacancy by bombarding high energy atom to the graphene surface, then placing a metal atom in the vacancy site, the strong interaction between surface and atom plays important role for SAC to achieve stability and high activity [28]. Earlier investigations on graphene as a supporting material for heterogeneous catalysts for example Cu and Fe doped graphene [7, 15] showed high activity towards CO oxidation.

Recently, other 2D materials, particularly transition metal dichalcogenides (TMDs), such as molybodenum disulfide (MoS_2) has attracted a great attention due to its unique physical, electrical and optical properties [29–31]. Researchers have found the growth of the high quality MoS_2 [32, 33] and proposed a wide variety of applications for instance hydrogen evolution reaction [34], sensors [9, 35, 36], lithium ion batteries [37]. MoS_2 monolayer consists of three atomic layers : a Mo layer sandwiched between two S layers. Like the graphene, MoS_2 is also chemically inert as it has no dangling bond in its basal plane, therefore, S atoms are expected not to be chemically active. Creation of S vacancy controllably and embedding a metal atom at the vacancy site or introducing a dopant atom could provide a facile route for the basal plane to be catalytically active. Because of charge transfer and atomic orbital hybridization, the interaction between the metal and substrate plays a significant role in determining catalytic activity . For CO oxidation, past studies Al-doped MoS_2 [6], Fe-embeded MoS_2 [38] have proved the competency of single atom supported MoS_2.

Chapter 2

First-principles Methods

2.1 Introduction

We are going to discuss density functional theory (DFT) which has been implemented throughout our calculations within the framework of Vienna ab-initio simulation package (VASP). It has gained enormous popularity since the last quarter of 2000 in the field of computational materials science, condensed matter physics, computational nanochemistry etc. for its great efficiency saving huge amounts of computation time. The ground state properties of many-body systems are investigated employing the ab-initio approximation. In earlier methods, the solutions of the electronic systems are too gruesome because of the electronic interaction which is quantum mechanical phenomena and the complexity increases with the increasing number of electrons in the system. However, DFT emerges bringing the solution of many body systems of interacting particles only by describing the ground state single particle density, $\rho(\vec{r})$, which describes all the information associated with ground state wave function of many body systems.

2.2 Schrodinger's equation for a many-body system

Quantum Mechanics [39] is the must use tool for predicting the electronic

structure of many body systems. Unlike the classical mechanics, we use the following schrodinger's equation in quantum mechanics for solutions,

$$\hat{H}\Psi_i(r_1, ..., r_n, R_1, ..., R_N) = E\Psi_i(r_1, ..., r_n, R_1, ..., R_N) \tag{2.1}$$

Where $\hat{H}$represents the hamiltonian operator, $\Psi_i$is the wave function of the ith state of the system which contains all the information of the system and E is the total energy of the system, r_1,...., r_n represent the spin and cartesian coordinates of the n electrons in the system, and R_1,.....,R_N are the nuclear coordinates of the N nuclei in the system. The Hamiltonian operator is given by,

$$\hat{H} = \hat{T}_{\mathrm{e}} + \hat{T}_{\mathrm{n}} + \hat{V}_{\mathrm{en}} + \hat{V}_{\mathrm{ee}} + \hat{V}_{\mathrm{nn}} \tag{2.2}$$

where the kinetic (T) and potential (V) energies of n electrons (e) and N nuclei (n) are given by,

$$\begin{aligned}
\hat{T}_{\mathrm{e}} &= -\frac{1}{2}\sum_{i=1}^{n}\nabla_i^2 \\
\hat{T}_{\mathrm{n}} &= -\frac{1}{2}\sum_{A=1}^{N}\frac{\nabla_A^2}{N_A} \\
\hat{V}_{\mathrm{en}} &= -\sum_{i=1}^{n}\sum_{A=1}^{N}\frac{Z_A e^2}{r_{iA}} \\
\hat{V}_{\mathrm{ee}} &= -\sum_{i=1}^{n}\sum_{j>i}^{n}\frac{e^2}{r_{ij}} \\
\hat{V}_{\mathrm{nn}} &= -\sum_{A=1}^{N}\sum_{B>A}^{N}\frac{Z_A Z_B e^2}{R_{AB}}
\end{aligned} \tag{2.3}$$

where, ∇^2 is the Laplacian operator, A and B represent N nuclei and i,j are n electrons in system. The first two terms are kinetic energy terms of electron and nuclei, respectively. Later three terms denote electron-nuclei, electron-electron, and nuclei-nuclei interaction, respectively.

There are different approximations for the solution of equation (2), such

as Born-Oppenheimer approximation [40] which allows us to seperate the motions of the electron and nuclei. The mass of the nuclei is ~10^3heavier than the electrons. As a consequence, the motion of the nuclei is much slower than electrons and treated as classically. After exclusion of nuclei parts, the equation (2) becomes,

$$\hat{H}_e = -\frac{1}{2}\sum_{i=1}^{n}\nabla_i^2 - \sum_{i=1}^{n}\sum_{A=1}^{N}\frac{Z_A e^2}{r_{iA}} - \sum_{i=1}^{n}\sum_{j>i}^{n}\frac{e^2}{r_{ij}} \tag{2.4}$$

The solution of equation (1) using the electronic Hamiltonian of (eq.4) provides the electronic wave function and total electronic energy. Then, adding the nuclei-nuclei interaction with the new solution can give the total energy. However, even after simplifying the Schrodinger equation the challenge remains for finding the solution of the wave function as the number of the electrons are in the order of ~10^{23} and the complexity of finding the electron correlation energy.

2.3 Density functional theory (DFT)

DFT mainly originated by Hohenberg & Kohn providing the two theorems in the year of 1964 [41]. According to their theorems the ground state energy of a system of interacting electrons in an external potential is a functional of the electron density, $\rho(\vec{r})$:

$$E[\rho(\mathrm{r})] = \int \rho(\mathrm{r}) V_{ext}(\mathrm{r}) d\mathrm{r} + F[\rho(\mathrm{r})] \tag{2.5}$$

Where $F[\rho(\vec{r})]$ is a functional of the electron density $\rho(\vec{r})$, $V_{ext}(\vec{r})$ is the external potential. The Hohenberg-Kohn theorems are powerful. The ground state energy can be determined by minimizing the equation (5). Nevertheless, in practice the complexity remains for computing the ground-state density of a system.

2.4 The Kohn-Sham Formulation

Kohn and Sham introduced the exchange-correlation [42] term by expanding the functional term $F[\rho(\vec{r})]$. To produce reasonably accurate values for properties like geometries, work functions, adsorption energies, bonding energies etc., approximations of functionals had been made with constraint. The universal functional $F[\rho(\mathrm{r})]$ was then separated into three terms,

$$F[\rho(\mathrm{r})] = T[\rho(\mathrm{r})] + E_{\mathrm{H}}[\rho(\mathrm{r})] + E_{\mathrm{xc}}[\rho(\mathrm{r})], \tag{2.6}$$

where $T[\rho(\mathrm{r})]$ is the kinetic energy of a non-interacting electron gas of density $\rho(\vec{r})$, $E_{\mathrm{H}}[\rho(\mathrm{r})]$ is the classical electrostatic (Hartree) energy of the electrons,

$$E_{\mathrm{H}}[\rho(\mathrm{r})] = \frac{1}{2}\iint \frac{\rho(\mathrm{r})\rho(\mathrm{r}')}{|\mathrm{r}-\mathrm{r}'|} d^3\mathrm{r} d^3\mathrm{r}', \tag{2.7}$$

and $E_{\mathrm{XC}}[\rho(\mathrm{r})]$ is the exchange-correlation energy. Kohn and Sham expressed the charge density, $\rho(\vec{r})$ in terms of a set of single particle orthonormal states, such that

$$\rho(\mathrm{r}) = \sum_{i=1}^{N} |\psi_i(\mathrm{r})|^2, \tag{2.8}$$

where N is the number of particles in the system. Then kinetic energy $T[\rho(\mathrm{r})]$ of the system is given by,

$$T[\rho(\mathrm{r})] = -\frac{1}{2}\sum_{i=1}^{N} \int \psi_i^*(\mathrm{r})\nabla^2\psi_i(\mathrm{r}) d^3\mathrm{r}. \tag{2.9}$$

Here, $T[\rho(\vec{r})]$is not a true kinetic energy term for interacting electrons in the system rather it is the kinetic energy of N number of non-interacting particles which are called Kohn-Sham particles. The exchange-correlation part contains the difference between this energy and true electronic energy. Similarly, the single particle Kohn-Sham wave equations can be reconstructed

from the rest of the energy terms of the equation 2.6. Now, the solution of the Schrodinger equation becomes tractable by expressing the total energy of the system in terms of single particle wave function, however the exchange-correlation part is still unspecified.

2.5 Approximations for the Exchange-Correlation Functional

2.5.1 Local Density Approximation (LDA)

In solid state calculations, one of the common approximations to $E_{\mathrm{xc}}[\rho(\mathrm{r})]$ is the local density approximation (LDA) which is based on the assumption that the exchange-correlation energy of a system at a given point is dependent on the electron density of that particular point of the system. A localized region of a molecule behaves like a uniform electron gas as it is assumed that the charge density varies slowly throughout the molecule. If E_{xc} is the exchange-correlation energy per particle in the uniform electron gas model then the total exchange-correlation energy for the system can be determined by taking the integration over all space,

$$E_{\mathrm{xc}}^{\mathrm{LDA}}[\rho(\mathrm{r})] = \int d^3\mathrm{r}\varepsilon_{\mathrm{xc}}^{\mathrm{hom}}(\rho(\mathrm{r}))\rho(\mathrm{r}), \tag{2.10}$$

where $\varepsilon_{\mathrm{xc}}^{\mathrm{hom}}(\mathrm{r})$ the exchange-correlation energy per particle of a homogeneous electrons gas having the same local density $\rho(\mathbf{r})$ as the inhomogeneous system at point $\mathbf{r}$. For atoms, molecules, clusters, surfaces, and interfaces, the LDA is fairly accurate and produces good results. However, LDA failed to describe the properties of the collective system such as dielectric constants, weak bonds. The binding energies are overestimated, on the other hand, the atomic ground state energies and ionization energies are underestimated.

2.5.2 Generalised Gradient Approximation (GGA)

To overcome the limitation of LDA, GGA was introduced. Using the gradient of density at a particular point $\vec{r}$ the LDA results can be modified. In GGA, the gradient of the electron density and the density itself are responsible for the exchange-correlation energy,

$$E_{\mathrm{xc}}^{\mathrm{GGA}}[\rho(r)] = \int d^3 r \varepsilon_{xc}^{GGA}(\rho(r), \nabla\rho(r), ...)\rho(r) \tag{2.11}$$

GGA functionals are clearly better suited to reflect inhomogeneity in the electron density than LDA functionals, and appear to produce more reliable total energies, atomisation energies, and structural energy differences by taking into account the spatial variation of the electron density. Unlike the LDA, the calculation of the energy for the exchange correlation can not be based upon an obvious reference System.

Among a great number of GGA functionals the most commonly used gradient approximation proposed by Perdew and Wang in 1991 [43]. The most recent modified form devised by Perdew, Burke and Ernzerhof known as PBE [44].

2.6 Plane wave pseudopotentials implementation of DFT

The practice of DFT calls for additional methods and approximations to be used, mainly for two reasons. There are an infinite number of interacting electrons in infinite periodic systems, such as crystals, each of whose wave function must be determined; additionally, the basis sets needed to expand these wave functions must be infinite. Because of these difficulties, the system is computationally infeasible. To overcome this problem, the use of the Bloch theorem and expansion of the wavefunctions in plane wave basis sets are useful.

2.6.1 Blöch's theorem

The crystal periodicity has been used in Bloch's theorem [45]. In a crystal, with the lattice translation operator the potential and electron charge density repeat. Within a periodic lattice the lattice-translation operator commutes with the one particle effective Hamiltonian. Thus, it is considered the Hamiltonian of a solid is periodically invariant. Hence, the wavefunction can be written as the product of a lattice periodic part $u_j(\mathrm{r})$ and a wavelike part $\mathrm{e}^{ik.r}$,

$$\psi_{j,\mathrm{k}}(\mathrm{r}) = u_j(\mathrm{r})\mathrm{e}^{i\mathrm{k}.\mathrm{r}}, \tag{2.12}$$

where the subscript j and $k$indicate the band index and a continuous wave vector that is confined to the first Brillouin zone of the reciprocal lattice, respectively. The function $u_j(\mathrm{r})$ has the same periodicity as the direct lattice. So, it can be expanded in terms of a discrete plane-wave basis set with wave vectors **G** that are reciprocal lattice vectors of the crystal, *i.e.*

$$u_j(\mathrm{r}) = \sum_{\mathrm{G}} C_j^G \mathrm{e}^{i\mathrm{G}.\mathrm{r}}, \tag{2.13}$$

where the wave vectors **G** are defined by $G_i.a_j$=$2\pi\delta_{ij}$, where $\vec{a}_j$ are crystal lattice vectors and C_j^G are the plane-wave coefficients. From this above two equations the wave functions can be expressed in terms of a linear combination of plane-waves,

$$\psi_{j,\mathrm{k}}(\mathrm{r}) = \sum_{\mathrm{G}} C_{j,\mathrm{k}}^G \mathrm{e}^{i(\mathrm{k}+\mathrm{G}).\mathrm{r}}. \tag{2.14}$$

Bloch theorem is very useful to reduce the problem of finding the infinite number of wave functions at an infinite number of k-points to finite number of wave functions at a finite number of k-points as wave functions do not vary much in the neighborhood of a k-point over the brillouin zone. Hence, the estimation of wave functions in a region of k-space is possible by only

sampling the wave functions at a single k-point.

2.6.2 Pseudopotentials

Explaining a plane wave basis set that contains all the electrons is quite impossible because it would require a huge number of wave functions corresponding to the number of electrons in a system for describing the oscillations at the core regions which subsequently increases the computational burden heavily. In case of pseudopotentials [46, 47], the core electrons along with the strong nuclear potential are replaced with a comparatively weaker and smoother pseudopotential and only the valence electrons are treated explicitly. The reduction of cut-off energies by using the pseudopotentials happens due to two reasons : first the high energy core electrons that need large basis set are removed , and second, the valence electrons are no need to be orthogonal to core electrons following pauli exclusion principle as the core electrons are removed.

As the number of electrons are reduced because of using the pseudopotentials has an advantage of making the computational cost lower. Nonetheless, the replacement of pseudopotentials in place of core electrons and nuclear potential changes the wave function and, as a consequence, it could lead to the poor representation of the electronic structure of the system. Therefore, only changing the wave function inside the core radius, and making the new and old potentials similar outside of the core region, can help to get rid of the above problem. It is necessary to include all the closest electrons to the nucleus in the core radius, although the effect of these filled shells electrons on the electronic system is little. There are some special cases where the core electrons contribute to the bonding of a system, even though these electrons are packed within a closed shell, so the core radius has to be chosen carefully.

2.6.3 PAW

On the contrary to the pseudopotential method, the core electrons are kept in a frozen state and the full all-electron valence wave functions are also considered. Similar to the pseudopotential method, inside the core radius the true wave functions are replaced by smooth wave functions. To obtain the true wave function from the smooth one a linear transformation operator can be formed. In the Projector Augmented-Wave Potentials (PAW) method, based on a linear transformation of the pseudo wave function $\tilde{\psi}$ to the all-electron wave function ψ :

$$|\psi_n\rangle = |\tilde{\psi}_n\rangle + \sum_i |\phi_i\rangle \langle \tilde{p}_i|\tilde{\psi}_n\rangle - \sum_i \left|\tilde{\phi}_i\right\rangle \langle \tilde{p}_i|\tilde{\psi}_n\rangle \tag{2.15}$$

with $\tilde{\psi}_n$ variational quantities. The index i refers to a sum over the atomic site, the angular momentum and reference energies. ϕ and $\tilde{\phi}$ are the all-electron and pseudo partial waves that match at the core radius. Finally, p_{i} are the projector functions that have to be created in a way to be dual to the partial waves:

$$\left\langle \tilde{p}_i|\tilde{\psi}_j\right\rangle = \delta_{ij} \tag{2.16}$$

Thus, the PAW method, implemented in VASP, works directly with the all-electron valence wave function and all-electron valence potentials.

2.7 Structure and properties calculation method

Here, we are going to discuss the general idea of some physical and chemical properties such as lattice constant, adsorption energy, energy barrier etc. that are calculated in this thesis.

2.7.1 Structural properties

The crystal structures can be presented in terms of unit cells of certain shapes and sizes because of their periodicity [48]. Corresponding to the edge lengths and angles between vectors and the shape of the lattice symmetry can be used to describe the size of the unit cell. The lattice constant is determined by the total energy minimization of the structure as a function of cell volume. The atomic positions inside the cell are presented by fractional coordinates relative to the unit cell.

2.7.2 Energy calculation

Adsorption is defined as the adhesion of molecules of gas, liquid, or dissolved solids to a surface [49]. Depending on how strong the interaction between the surface and adsorbate, adsorption can be categorized as physisorption, chemisorption or dissociative adsorption. The interaction is weak when the adsorbates adsorb physically on the surface. On the other hand, the interaction is strong in case of chemisorption and the electronic structure of the adsorbate is changed. The adsorption energy depends on various factors : distance between adsorbate and adsorbent, the characteristics of adsorbent and the substrate, on the degrees of freedom of corresponding atoms in the system. The adsorption energy is calculated according to the equation, in case of gas adsorption,

$$E_{ads} = E_{surface+gas} - E_{surface} - E_{gas} \tag{2.17}$$

where $E_{surface+gas}$, $E_{surface}$, and E_{gas} are the total energy of the entirely adsorbed system, of the slab, and the isolated gas molecules.

2.7.3 Nudge elastic band calculation with climbing image

To find the minimum energy path (MEP) of a system from its initial state (IS)

to final state (FS) i.e, from one stable configuration to another one, climbing image nudge elastic band (cNEB) method [50] is used. The cNEB method is very efficient for finding the highest saddle point on the potential energy surface which eventually gives the actual activation barrier of a reaction. The activation barrier or energy barrier is an important quantity for the reaction kinetics which is defined by the amount of energy required for a reaction to happen. The nature of a chemical reaction is to find the energetically lowest route that is termed as MEP to complete the reaction. There are several guess states that are considered as the initial band between IS and FS. Unlike the simple NEB method where a fictitious spring force is applied on each image (state) along the parallel direction to maintain an equal distance between the states, the highest energy image does not feel the spring forces in cNEB method as the true forces along the tangent are inverted. Therefore, the distance on either side of that image is different, and the image tries to maximize its energy along the band and minimize in all other directions to reach the saddle point. Once the energy convergence for finding the MEP is done locally the highest energy energy state or transition state (TS) is located and the activation barrier is calculated by comparing the binding energy of TS with IS.

2.8 Vienna ab-initio simulation package (VASP)

We performed the DFT calculations in this thesis using the Vienna ab-initio simulation package (VASP) [51, 52]. This DFT based program is designed for the systems of periodic boundary conditions. Pseudopotentials and plane wave basis set are used in this program. This program's internal structure consists of two major loops: inner electronic loop and outer ionic loop. Kohn-Sham equations are solved by implementing a self consistent algorithm in the inner loop. Beside that, the total force and energy are also determined. On the other hand, ionic movement, geometry optimization and

molecular dynamics algorithms are taken care of in the outer loop.

Chapter 3

Results and discussion

3.1 Computational details

Spin polarized density functional theory (DFT) has been implemented within the framework of Vienna ab initio simulation package (VASP) for this study [51, 52]. The exchange and correlation energy was calculated using the generalized gradient approximation (GGA) within the Perdew-Burke- Ernzerhof (PBE) functional [44]. An energy cut-off of 500 eV was used for the plane wave basis set. The Brillouin-zone integration k-mesh was sampled with 3×3×1 [53]. The energy and force convergence criteria were set 10^{-5} eV, 0.01 eV/Å, respectively. A 4×4 supercell of MoS_2 was considered as a supported material for doping the Ni atom to study the adsorption of gas molecules and CO oxidation. To avoid the interaction between MoS_2 sheets, the vacuum distance was kept 20 Å between the repeated layers along z-axis. All the atoms were free to move within the cell maintaining a constant shape and volume of the cell throughout the calculations. Gas molecules were placed on a standard distance of 3 Å from the surface along the z-direction in case of adsorption energy calculation. Climbing image nudge elastic band method was used to find the minimum energy path and the spring force between adjacent images was 5.0 eV/Å [50].

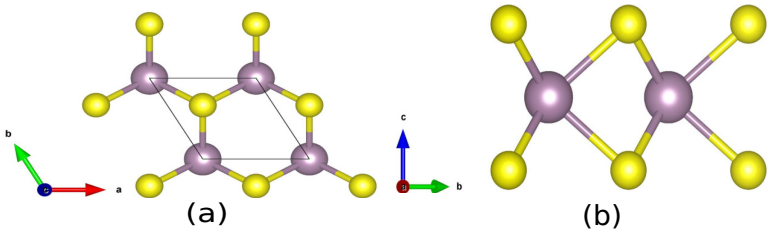

Figure 3.1: Schematic view of MoS_2unit cell (a) top view, (b) side view. Purple and yellow balls represent the Mo and S atoms, respectively.

3.2 Structural properties

We start with the stable 2H-MoS_2 unit cell. The coordination of 2H-MoS_2 is trigonal prismatic with hexagonal symmetry. The lattice constant of the unit cell is 3.18 Å, the thickness of the unit cell is 3.13 Å, the bond length between Mo and S atom is 2.41 Å, and bond angle of S-Mo-S is 80.79°, which have good agremeent with the experimental value [54] and with the theoretical value [55]. Then, we introduce a 4×4 supercell to simulate Ni-$MoS_2$where a Ni atom is doped for one S atom site per cell.

3.3 Screening the diffusion barrier

We first consider the non-noble metal atom Ni for the substitution with a superficial S atom on MoS_2 monolayer. It can be clearly seen (see IS of Figure 3.2) that Ni atom forms strong covalent bonds with its neighboring Mo atoms which can enhance the stability of the doping atoms on the substrate. The high binding energy 4.23 eV clearly showed the strong interaction between Ni atom and the MoS_2. Here, the binding energy is defined as E_b(Ni) = E_{tot}(Ni+MoS_2) - E_{tot}(MoS_2) - E_{tot}(Ni), where E_{tot}(Ni+MoS_2), E_{tot}(MoS_2), E_{tot}(Ni) are the total energy of the Ni doped MoS_2, total energy of MoS_2 with a S-vacancy, and total energy of an isolated Ni atom, respectively. The Ni atom protudes slightly upward from the S-plane after relaxation. The amount of charge is transferred from Ni atom to the sub-

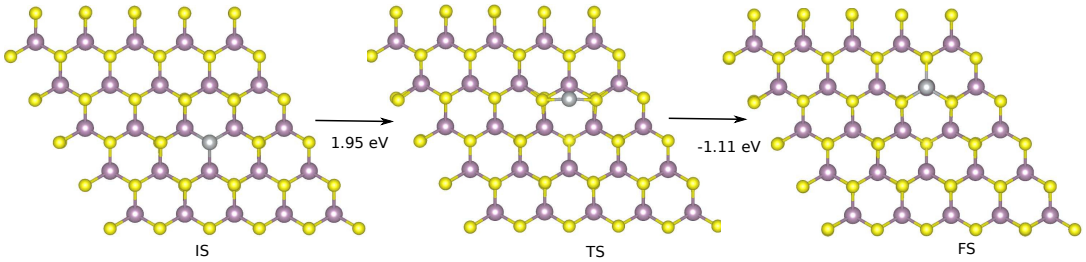

Figure 3.2: Energy barrier of the Ni atom from the doping site to its neighboring Mo top site. Here, IS, TS, FS are initial state, transition state, and final state, respectively, for the minimum energy path. Violet, yellow, gray color balls represent Mo, S, Ni atoms respectively.

strate is 0.06e, according to the Bader charge analysis [56], which can be verified by the pauli electronegativity scale where the Ni atom(1.91) is less electronegative compared to the Mo atom (2.16). The system becomes non-magnetic in spite of having the magnetic element Ni. Other than the vacancy site, we adsorbed Ni atom at different positions to find the most stable configuration. We found Ni atom at the top of the Mo site is the most stable. To make sure that the Ni atom doesn't create any clustering problem, we carefully determined the diffusion barrier of Ni atom from the vacancy site to its neighboring Mo top site (Figure 3.2). The nudge elastic band calculation gives the energy barrier of 1.95 eV, between these two configurations, which demonstrates that Ni atom bonded strongly at the doping site and excludes the clustering problem.

To better understand the Ni doped MoS_2, we plotted the charge density difference (CDD) and spin polarized local density of states (LDOS) of Ni and Mo atoms (Figure 3.3). CDD plot shows that the most of the charge is accumulated between the Ni and Mo bonds. The strong hybridization of Ni-3d orbital with 4d & 5p orbitals of Mo indicates the strong interaction between Ni and Mo atom, that effectively prevents the aggregation of Ni atom on MoS_2 surface. Moreover, this strong hybridization fulfills the non-bonding 3d states of Ni atom, which eliminates its magnetism.

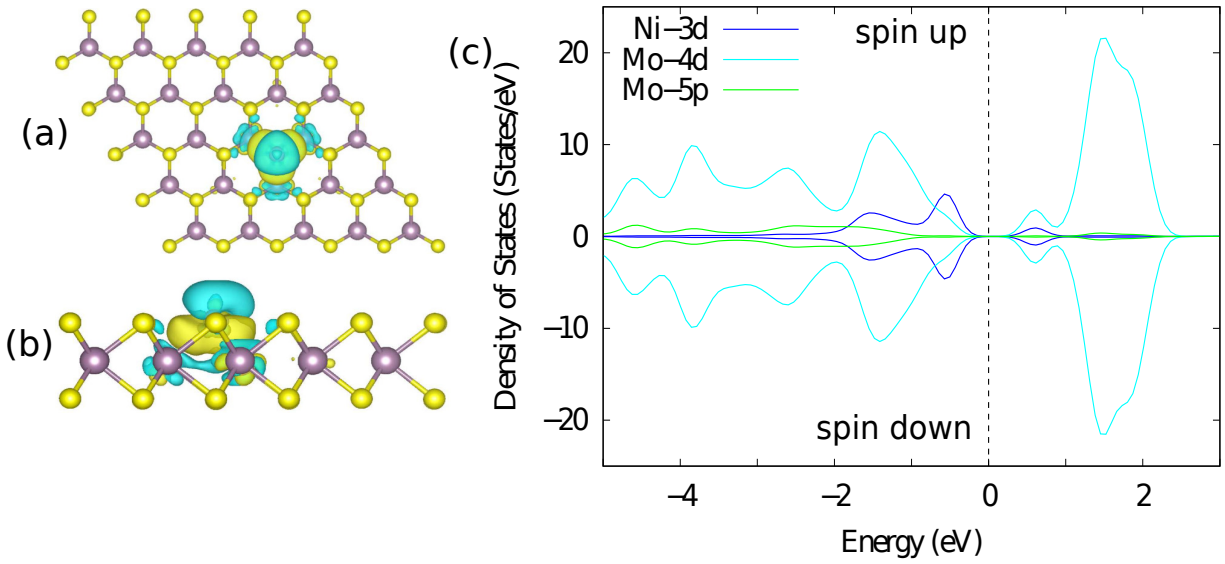

Figure 3.3: Charge density difference (a) top view, (b) side view (blue and yellow region represent the charge depletion and accumulation, resepectively; (c) spin polarized local density of states of Ni doped MoS_2

3.4 Adsorption of the gas molecules

On the beforehand of investigating the CO oxidation, we justify the adsorption of CO, O_2, O, CO_2 gas molecules on the Ni doped MoS_2 (Figure 3.4). We consider different configurations in order to find the energetically most favorable one for each adsorbate. Our study found, for CO adsorption, the most favorable is end-on configuration with adsorption energy 1.07 eV facing the C-end towards Ni atom. The Ni-C bond length is 1.84 Å, and the C-O bond length elongated slightly from 1.14 Å to 1.153 Å. On the other hand, O_2 favors side-on pattern with the E_{ad} value of 0.78 eV. The O-O bond of O_2 prolonged from 1.20 Å to 1.32 Å, which shows that the O-O bond is activated (Table 3.1).

The LDOS and CDD of CO and O_2 is shown Figure 3.5. Bader charge analysis shows Ni atom loses $0.31e$ amount of charge and O_2 gains $0.42e$. The CDD shows, in case of O_2 adsorption, the much of the charge is accumulated around O_2, which mainly occupied by the O_2-$2\pi^*$ antibonding

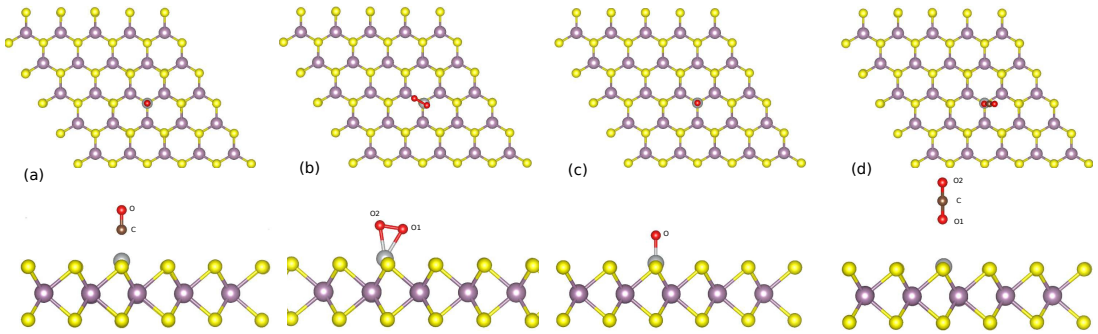

Figure 3.4: Most favorable adsorption sites for (a) CO, (b) O_2,(c) O, (d) CO_2 gas molecules. The upper and lower panel shows the top and side views, respectively.

Table 3.1: Adsorption energy, charge transfer and bonding details of different adsorbates on Ni-MoS_2

Adsorbates	E_{ad} (eV)	Charge transfer (e)	Bonding details	
			Bond	Distance (Å)
CO	1.07	0.14	C-O	1.153
			Ni-C	1.84
O_2	0.78	0.42	O-O	1.32
			Ni-O1	1.91
			Ni-O2	1.96
O	3.32	0.61	Ni-O	1.65
CO_2	0.23	0.01	Ni-O1	2.77
			O1-C	1.18
			C-O2	1.17

orbital resulting bond elongation (see Figure 3.5 c and d). The significant hybridization can be seen between Ni-O_2 (see Figure 3.5f). According to the above findings, it is highly likely that Ni-MoS_2 can activate O_2 towards CO oxidation. On contrary, only 0.14e amount of charge is transferred from substrate to CO, mostly gathered in Ni-C interface (see Figure 3.5 a and b). There is no remarkable hybridization between Ni-CO indicates that the positively charged Ni atom help to weaken the CO adsorption to facilitate the O_2 adsorption. The single O atom can be adsorbed stably with a higher adsorption energy of 3.32 eV. The low adsorption energy of CO_2 shows the weak interaction and easy desorption from surface.

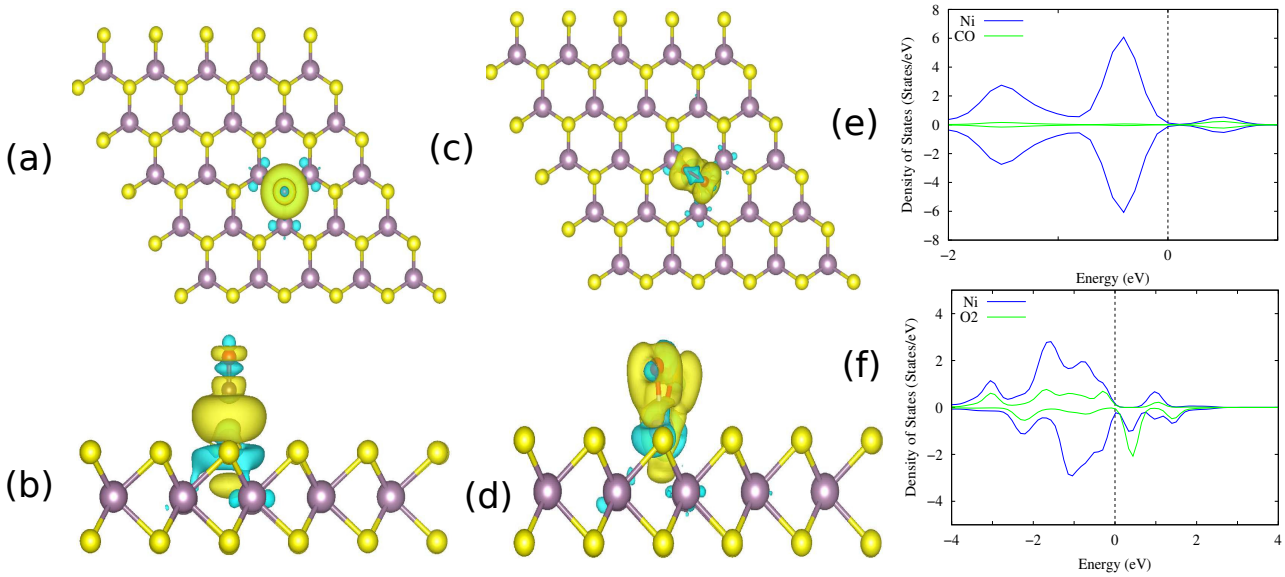

Figure 3.5: Charge density difference of CO (a) top, (b) side views ; O_2(c) top, (d) side views. The yellow and green regions in CDD represent charge accumulation and depletion, respectively. Spin-polarized local density of states (e) CO on Ni-MoS_2, (f) O_2 on Ni-MoS_2

3.5 Mechanism for CO oxidation

There are two well established mechanisms for CO oxidation reactions: 1) Langmuir-Hinshelwood (LH) mechanism, 2) Eley-Rideal (ER) mechanism. In case of LH mechanism, the co-adsorption of CO and O_2 gas molecules on the catalyst is considered as starting point before reaction. Then, a terminal O atom approaches to CO to form a transition state (TS). Finally, the desorption of produced CO_2 molecule is considered as final step following OOCO peroxide-type intermediate state. The remaining O atom is adsorbed on Ni atom to take part into reaction on the next step. However, ER mechanism starts off with direct reaction between CO gas molecules and pre-adsorped O_2 molecules on the surface and formed carbonate-like CO_3 intermediate state before producing CO_2 molecule.

3.5.1 ER (Eley-Rideal) mechanism

In case of ER mechanism, we found that the intermediate state (formation of carbonate like CO_3 state) is energitically 0.70 eV more stable than the final product (physisorbed CO_2 and chemisorbed atomic O). So, the reaction is

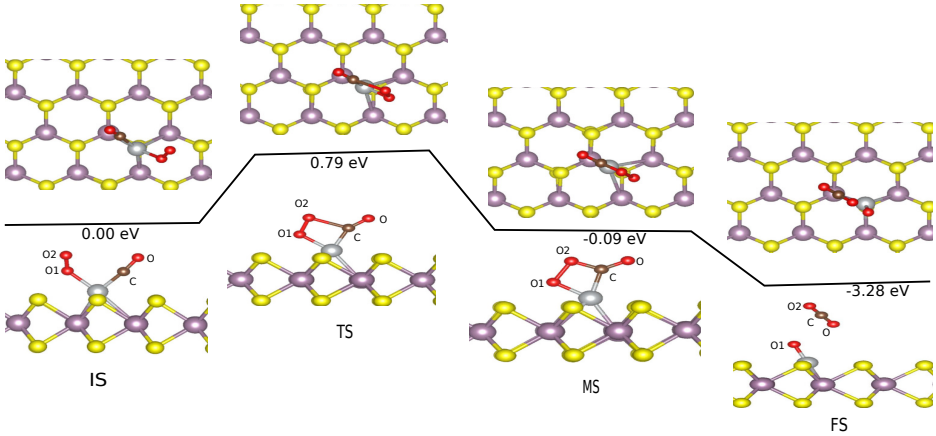

Figure 3.6: MEP for LH mechanism. Upper and lower panels represent top and side views, respectively.

endothermic and thermodynamically not favorable.

3.5.2 LH (Langmuir-Hinshelwod) mechanism

To make sure that the reaction process does happen on Ni-MoS_2 via LH mechanism, we tested by keeping the CO and O_2 in the vicinity of the catalyst and the formation of the OOCO type complex state was observed after geometry optimization. This indicates that the LH mechanism is possible on Ni-MoS_2. The most favorable configuration of coadsorption of CO and O_2 is considered as initial state (IS) for finding the minimum energy path (MEP). Both the CO and O_2 are in a tilting position on the surface. In the final state (FS), CO_2 is formed and physisorbed with an atomic O chemisorbed on Ni-MoS_2. The local configurations and structural parameters of different states are displayed in Figure 3.6 and Table 3.2 (a) .

Passing over the initial state to the transition state, the O-O bond of adsorbed O_2 is elongated from 1.27 Å 1.35 Å, while the C-O bond of CO changes slightly from 1.15 Å to 1.17 Å. In the meanwhile, one terminal atom from O-O bond approaches to CO to form a OOCO peroxide-type intermediate state (MS) enlarging the bond length of O-O to 1.55 Å and C-O

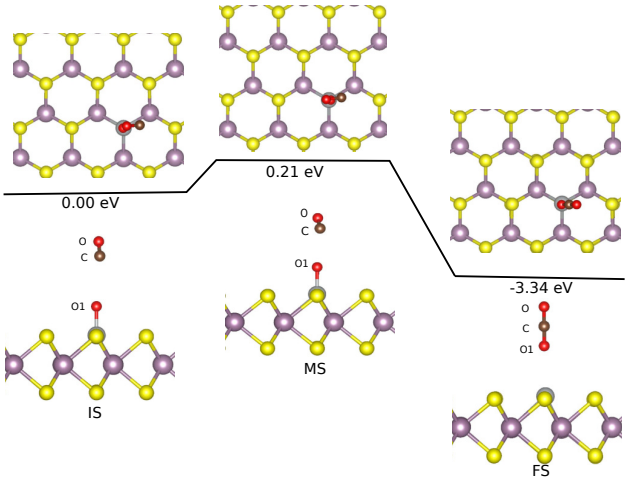

Figure 3.7: Atomic configurations along the MEP for ER mechanism.

Table 3.2: Structural parameters of different states along MEP for CO oxidation on Ni-MoS_2

(a) Bond	Distance (Å)			
	IS	TS	MS	FS
Ni-O1	1.97	1.90	1.82	1.65
Ni-C	1.83	1.97	1.94	4.25
C-O	1.15	1.17	1.20	1.17
O1-O2	1.27	1.35	1.55	3.38
C-O2	2.93	1.78	1.32	1.17

(b) Bond	Distance (Å)		
	IS	MS	FS
Ni-O1	1.61	1.62	2.24
O1-C	2.99	2.40	1.18
C-O	1.14	1.15	1.17

to 1.20 Å. The energy barrier from IS to TS is 0.79 eV with an exothermic reaction energy of 0.09 eV. Then in the final state, one CO_2 is formed releasing 3.28 eV energy to become the most stable in its form. The remaining O atom can stably adsorbed on the surface with an adsorption energy of 3.32 eV.

We further investigated ER mechanism for CO oxidation by the pre-adsorbed O atom. Configurational details are presented in Table 3.2 (b) and shown in Figure 3.7. The adsorption of CO over the pre-adsorbed O atom is considered as IS. The distance between C-O1 is 2.99 Å. The CO molecule approaches towards O atom facing a low energy barrier of 0.21 eV. The formation of CO_2 is an exothermic reaction where the amount of energy is released by the system is 3.38 eV. Consequently, the surface becomes free from any adsorbed gas molecules and ready to repeat the process in a continuous manner.

Chapter 4

Summary

In summary, we performed first principles calculations to investigate CO, carbon monoxide, oxidation on Ni doped MoS_2. Doping a non noble metal atom Ni on the substrate enhance the stability of single atom catalyst with a high diffusion barrier of 1.95 eV. Our study found that the CO oxidation takes place on Ni-MoS_2 via LH mechanism with a low activation barrier of then followed by the ER mechanism forming CO_2, carbon dioxide, showing a superior catalytic behavior. This study suggests that the doping a metal atom to a chemically inert surface like MoS_2 could be useful for catalytic reactions.

Bibliography

[1] A. Corma, Angewandte Chemie International Edition **46**, 7734 (2007).

[2] L. Yuwen, F. Xu, B. Xue, Z. Luo, Q. Zhang, B. Bao, S. Su, L. Weng, W. Huang, and L. Wang, Nanoscale **6**, 5762 (2014).

[3] A. Alavi, P. Hu, T. Deutsch, P. L. Silvestrelli, and J. Hutter, Physical Review Letters **80**, 3650 (1998).

[4] C. Du, H. Lin, B. Lin, Z. Ma, T. Hou, J. Tang, and Y. Li, Journal of Materials Chemistry A **3**, 23113 (2015).

[5] B. L. M. Hendriksen and J. W. M. Frenken, Physical Review Letters **89**, 046101 (2002).

[6] D. Li, W. Li, and J. Zhang, Applied Surface Science **484**, 1297 (2019).

[7] Y. Li, Z. Zhou, G. Yu, W. Chen, and Z. Chen, The Journal of Physical Chemistry C **114**, 6250 (2010).

[8] F. Li, J. Zhao, and Z. Chen, The Journal of Physical Chemistry C **116**, 2507 (2012).

[9] D. Ma, W. Ju, T. Li, X. Zhang, C. He, B. Ma, Z. Lu, and Z. Yang, Applied Surface Science **383**, 98 (2016).

[10] S. Huang, K. Hara, and A. Fukuoka, Energy & Environmental Science **2**, 1060 (2009).

[11] Y. Tang, L. Pan, W. Chen, C. Li, Z. Shen, and X. Dai, Applied Physics A **119**, 475 (2015).

[12] L. Zhou, A. Kandratsenka, C. T. Campbell, A. M. Wodtke, and H. Guo, Angewandte Chemie International Edition **58**, 6916 (2019).

[13] Y. Zhou, Z. Wang, and C. Liu, Catalysis Science & Technology **5**, 69 (2015).

[14] X. Zhang, Z. Yang, and R. Wu, Nanoscale **10**, 4753 (2018).

[15] E. H. Song, Z. Wen, and Q. Jiang, The Journal of Physical Chemistry C **115**, 3678 (2011).

[16] "CO Oxidation on Pd(100) and Pd(111): A Comparative Study of Reaction Pathways and Reactivity at Low and Medium Coverages | Journal of the American Chemical Society," .

[17] I. Nakai, H. Kondoh, T. Shimada, A. Resta, J. N. Andersen, and T. Ohta, The Journal of Chemical Physics **124**, 224712 (2006).

[18] F. Cosandey and T. E. Madey, Surface Review and Letters **08**, 73 (2001).

[19] M. Haruta, N. Yamada, T. Kobayashi, and S. Iijima, Journal of Catalysis **115**, 301 (1989).

[20] V. Matolín, M. H. Elyakhloufi, K. Mašek, and E. Gillet, Catalysis Letters **21**, 175 (1993).

[21] G. Krenn, I. Bako, and R. Schennach, The Journal of Chemical Physics **124**, 144703 (2006).

[22] M. S. Chen, Y. Cai, Z. Yan, K. K. Gath, S. Axnanda, and D. W. Goodman, Surface Science **601**, 5326 (2007).

[23] Y. Tang, X. Dai, Z. Yang, L. Pan, W. Chen, D. Ma, and Z. Lu, Physical Chemistry Chemical Physics **16**, 7887 (1393).

[24] H. Ha, H. An, M. Yoo, J. Lee, and H. Y. Kim, The Journal of Physical Chemistry C **121**, 26895 (2017).

[25] N. Lopez, T. V. W. Janssens, B. S. Clausen, Y. Xu, M. Mavrikakis, T. Bligaard, and J. K. Nørskov, Journal of Catalysis **223**, 232 (2004).

[26] "Single-atom catalysis of CO oxidation using Pt 1 /FeO x | Nature Chemistry," ().

[27] A. Junkaew, J. Meeprasert, B. Jansang, N. Kungwan, and S. Namuangruk, RSC Advances **7**, 8858 (2017).

[28] H. Wang, Q. Wang, Y. Cheng, K. Li, Y. Yao, Q. Zhang, C. Dong, P. Wang, U. Schwingenschlögl, W. Yang, and X. X. Zhang, Nano Letters **12**, 141 (2012).

[29] A. Splendiani, L. Sun, Y. Zhang, T. Li, J. Kim, C.-Y. Chim, G. Galli, and F. Wang, Nano Letters **10**, 1271 (2010).

[30] K. F. Mak, C. Lee, J. Hone, J. Shan, and T. F. Heinz, Physical Review Letters **105**, 136805 (2010).

[31] Y. Li, Z. Zhou, S. Zhang, and Z. Chen, Journal of the American Chemical Society **130**, 16739 (2008).

[32] Y.-H. Lee, X.-Q. Zhang, W. Zhang, M.-T. Chang, C.-T. Lin, K.-D. Chang, Y.-C. Yu, J. T.-W. Wang, C.-S. Chang, L.-J. Li, and T.-W. Lin, Advanced Materials **24**, 2320 (2012).

[33] K.-K. Liu, W. Zhang, Y.-H. Lee, Y.-C. Lin, M.-T. Chang, C.-Y. Su, C.-S. Chang, H. Li, Y. Shi, H. Zhang, C.-S. Lai, and L.-J. Li, Nano Letters **12**, 1538 (2012).

[34] L. A. King, W. Zhao, M. Chhowalla, D. J. Riley, and G. Eda, Journal of Materials Chemistry A **1**, 8935 (2013).

[35] V. Babar, H. Vovusha, and U. Schwingenschlögl, ACS Applied Nano Materials **2**, 6076 (2019).

[36] S. Zhao, J. Xue, and W. Kang, Chemical Physics Letters **595–596**, 35 (2014).

[37] Y. Li, D. Wu, Z. Zhou, C. R. Cabrera, and Z. Chen, The Journal of Physical Chemistry Letters **3**, 2221 (2012).

[38] D. Ma, Y. Tang, G. Yang, J. Zeng, C. He, and Z. Lu, Applied Surface Science **328**, 71 (2015).

[39] F. Jensen, *Introduction to Computational Chemistry* (2017).

[40] M. Born, J. R. Oppenheimer, and A. Physik, .

[41] P. Hohenberg and W. Kohn, Physical Review **136**, B864 (1964).

[42] W. Kohn and L. J. Sham, Physical Review **140**, A1133 (1965).

[43] J. P. Perdew and Y. Wang, Physical Review B **45**, 13244 (1992).

[44] J. P. Perdew, K. Burke, and M. Ernzerhof, Physical Review Letters **78**, 1396 (1997).

[45] N. W. Ashcroft and N. D. Mermin, *Solid State Physics* (2011).

[46] J. C. Phillips, Physical Review **112**, 685 (1958).

[47] J. C. Phillips and L. Kleinman, Physical Review **116**, 287 (1959).

[48] P. L. Taylor and O. Heinonen, *A Quantum Approach to Condensed Matter Physics* (2002).

[49] R. K. Brandt, M. R. Hughes, L. P. Bourget, K. Truszkowska, and R. G. Greenler, Surface Science **286**, 15 (1993).

[50] G. Henkelman, B. P. Uberuaga, and H. Jónsson, The Journal of Chemical Physics **113**, 9901 (2000).

[51] G. Kresse and J. Furthmüller, Computational Materials Science **6**, 15 (1996).

[52] G. Kresse and J. Furthmüller, Physical Review B **54**, 11169 (1996).

[53] H. J. Monkhorst and J. D. Pack, Physical Review B **13**, 5188 (1976).

[54] P. Joensen, E. D. Crozier, N. Alberding, and R. F. Frindt, Journal of Physics C: Solid State Physics **20**, 4043 (1987).

[55] "Single-Layer MoS2 with Sulfur Vacancies: Structure and Catalytic Application | The Journal of Physical Chemistry C," ().

[56] G. Henkelman, A. Arnaldsson, and H. Jónsson, Computational Materials Science **36**, 354 (2006).